Acta Cryst. (1988). A44, 22-25

Multiple Scattering and the 200 Reflection in Silicon and Germanium*

BY J. Z. TISCHLER AND J. D. BUDAI

Solid State Division, Oak Ridge National Laboratory, Oak Ridge, Tennessee 37831, *USA*

G. E. ICE

Metals and Ceramics Division, Oak Ridge National Laboratory, Oak Ridge, Tennessee 37831, *USA*

AND A. HABENSCHUSS

Oak Ridge Associated Universities, Oak Ridge, Tennessee 37830, *USA*

(*Received* 17 *May* 1987; *accepted* 30 *July* 1987)

Abstract

Absolute measurements of the 200 reflection in Si and Ge at various azimuthal orientations are compared with N-beam calculations of the integrated intensity. All of the non-zero integrated intensity is accounted for by multiple-beam scattering. The measurements match the calculations on the assumption that $F_{200} = 0$.

I. Introduction

Recent indications of a possible non-zero structure factor for the silicon 200 reflection (Post & Ladell, 1987) pose an interesting question since, for reasons of symmetry, the 200 structure factor F_{200} in diamond-structure materials should be exactly zero (Henry & Lonsdale, 1952). To investigate this problem we have made measurements of the 200 reflection in silicon and germanium using the ORNL X-ray beam line (X-14) at the National Synchrotron Light Source (NSLS) at Brookhaven National Laboratory.

Silicon and germanium 200 rocking curves were measured at various azimuthal orientations and analyzed using dynamical-theory multiple-beam calculations. The multiple-beam calculations included hundreds of extra reciprocal-lattice points to ensure that all multiple-beam effects were included. In this paper the measured rocking curves are completely accounted for by multiple-beam diffraction with a null 200 structure factor.

II. Multiple-beam scattering

The 200 reflection for the diamond structure is a basis-forbidden reflection. Most basis-forbidden reflections do not have precisely zero intensity owing to the existence of non-centrosymmetric parts in the atomic charge distribution; the atoms are not perfect spheres. These non-centrosymmetric parts, arising from the tetrahedrally oriented lobes of bonding electrons and the anharmonic core vibrations, produce a non-zero structure factor F_{hkl} for the 222, 442, 622 and other basis-forbidden reflections (Dawson, 1967). On the other hand, for any atomic charge distribution that is consistent with the tetrahedral site symmetry, the 200 structure factor is exactly zero. The null value of F_{200} is not the low-order result of an expansion; it is correct for all atomic charge distributions that are consistent with the atomic site symmetry. This is shown by the selection rules listed for the diamond cubic space group in *International Tables for X-ray Crystallography* (Henry & Lonsdale, 1952). If h, k or l are zero and $h + k + l$ is not evenly divisible by four, then $F_{hkl} = 0$. If F_{200} were found to be non-zero, then the material could not truly have the diamond cubic structure. Such a finding would, of course, affect many of the fundamental studies of silicon and germanium.

In general, the width of a reflection from a perfect crystal of material such as silicon and germanium is governed by the conservation of energy and the conservation of crystal momentum. The latter condition requires that the wave vector of the scattered beam be near a reciprocal-lattice point, and the former condition that the wave vector lie on the Ewald sphere.

Consider the situation shown in Fig. 1 where $\mathbf{k}_f - \mathbf{k}_0$ is exactly $\mathbf{H} = (hkl)$, and there is another reciprocal-lattice point $\mathbf{H}' = (h'k'l')$ off the Ewald sphere. H'' is a third reciprocal-lattice vector which is $\mathbf{H} - \mathbf{H}'$. We know from the definition of a lattice that if $\mathbf{H}$ and $\mathbf{H}'$ are reciprocal-lattice vectors then $\mathbf{H}''$ must also be one.

A reflection with final wave vector $\mathbf{k}'$ is clearly forbidden since $\mathbf{k}'$ is off the Ewald sphere and so the process does not conserve energy. However, the double process $\mathbf{k}_0 \rightarrow \mathbf{k}' \rightarrow \mathbf{k}_f$ is possible since $\mathbf{H}' + \mathbf{H}'' = \mathbf{H} = \mathbf{k}_f - \mathbf{k}_0$, and $\mathbf{k}_f$ is on the Ewald sphere. Note that the scattering is not a sequential process; there is no photon with wave vector $\mathbf{k}'$. The incident beam

* Research sponsored by the Division of Materials Sciences, US Department of Energy under contract DE-AC05-840R21400 with Martin Marietta Energy Systems, Inc.

0108-7673/88/010022-04$03.00

simultaneously uses $\mathbf{H}'$ and $\mathbf{H}''$ to scatter into the $\mathbf{k}_f$ direction.

This simultaneous process is very similar to a virtual transition in atomic physics where an excited state that cannot decay directly to a lower energy state, because of some selection rule, will instead decay through a still higher energy state. This analogy is the origin of the team 'virtual Bragg scattering' (Chapman, Yoder & Colella, 1981).

Let us also consider what the width of an allowed dynamical reflection will be. For directions in k space parallel to the crystal face, the incoming photon interacts with many rows of atoms. Thus the k-space width of the reflection in the plane parallel to the crystal face is given by the limitations on the beam coherence. In the direction normal to the crystal face, the width of the scattering in k space is given by the mean number of planes a photon samples before being scattered.

For a kinematic reflection involving a single very small crystallite, the number of planes is determined by the size of the crystallite. For a strong dynamical reflection the number of planes sampled is determined by the self-extinction length, since the beam is reflected out before it can see the back of the crystal. For a weak dynamical reflection, the penetration of the beam is limited by secondary extinction (absorption) rather than primary extinction. Thus the extent of the scattering in k space is approximately one inverse absorption length. This is more sharply peaked about $\mathbf{H}$ than the scattering from a strong dynamical reflection, since primary extinction is stronger than secondary extinction for a strong reflection. This view still holds for a weak multiple reflection regardless of $F_{\mathbf{H}}$. Thus the width of a rocking curve from weak multiple-beam scattering is indistinguishable from the width from weak two-beam scattering.

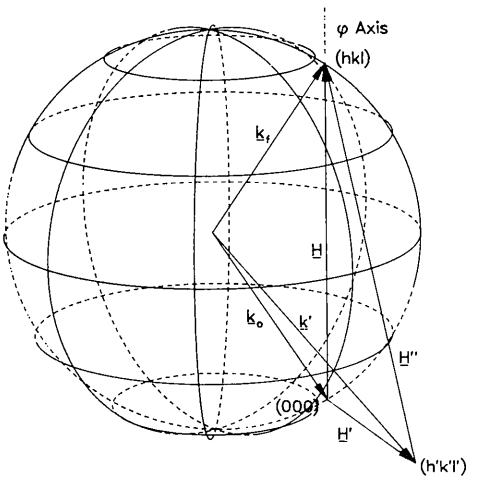

Fig. 1. The scattering geometry showing the incident and outgoing beams. Also shown are three reciprocal-lattice vectors, $\mathbf{H}$, $\mathbf{H}'$ and $\mathbf{H}''$. The φ axis is parallel to $\mathbf{H}=200$ and normal to the [010] direction (not shown). Note that the Bragg angle is independent of φ.

Since the effect of a strong allowed reflection far from the Ewald sphere may be as great as a weak forbidden reflection on the Ewald sphere (Tischler & Batterman, 1986), many extra reciprocal-lattice points must be included to determine correctly the magnitude and phase of very weak dynamical reflections. Fortunately, since the scattering is weak, an approximation (Tischler & Batterman, 1986; Shen, 1986) may be used which allows one to calculate with hundreds of beams using only a modest computer.

The central assumption in both the perturbation expansion of Shen (1986) and the approximation scheme used here (Tischler & Batterman, 1986) is that the scattering is weak; the reflectivity $\ll 1$. The Darwin development of dynamical diffraction has the X-ray beam repeatedly scattering back and forth from every plane in the crystal. However, as the interaction becomes very weak, an X-ray beam once scattered into the $\mathbf{k}_f$ direction has a negligible probability of later scattering out of the $\mathbf{k}_f$ direction. This is why the dynamical equations for weak interaction and strong absorption reduce to the kinematical expressions.

For weak multiple-beam diffraction a similar viewpoint prevails; once the beam diffracts into the $\mathbf{k}_f$ direction (now a second-order process) it leaves the crystal. There is no need to continue to calculate all possible rescattering. This result effectively decouples the multiple-beam scattering from F_{200}. Since the multiple-scattering contribution is not multiplied by F_{200}, the total scattered amplitude does not vanish as F_{200} goes to zero.

III. Measurements

The experimental measurements were carried out on the X-14 X-ray diffraction beam line at the National Synchrotron Light Source. The white radiation was reflected from a cylindrically bent mirror for harmonic rejection and vertical focusing, then by a double-crystal monochromator, and finally arrived at a diffractometer. The second crystal of the monochromator was sagittally bent to provide horizontal focusing. Both the mirror and the monochromator crystal were adjusted to produce a parallel X-ray beam and hence the sharpest possible rocking curves and multiple reflection peaks.

The mirror angle was set between the critical angles of the fundamental and harmonic from the monochromator. However, a few hundred counts per second remained in the 400 reflection when the 200 was set to diffract the fundamental wavelength. This signal was very useful as an alignment check to ensure that we were indeed at the correct Bragg angle, particularly when the 200 reflection was very weak. The final detector, a proportional counter, clearly

separated the fundamental from the harmonic at these low count rates, so the 200 rocking curves were not contaminated by the 400 reflection.

All of the rocking curves, for both the 400 and 200 reflections, were the same width, ~10″ arc for silicon and ~60″ arc for germanium. These widths correspond to the convolution of the intrinsic width (3·5″ arc for Si and 9·7″ arc for Ge) with the vertical beam divergence. The large rocking-curve widths come primarily from the mirror curvature, which is different for the silicon and germanium data. Although a large width reduces the signal-to-noise ratio, it does not affect the integrated intensity.

The data were collected as rocking curves at the position of the 200 reflection. These rocking curves were converted into integrated intensities by using an ion chamber as an absolute intensity monitor. The ion chamber was calibrated at each energy by use of a PIN diode to compare counts per second into the proportional counter with the direct beam. The PIN diode is one of the few devices with sufficient dynamic range to measure both a diffracted beam (10^4 counts s^{-1}) and the direct beam (10^{10} counts s^{-1}).

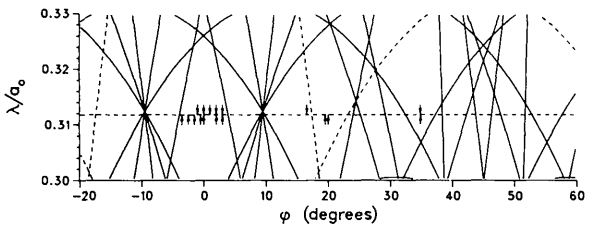

Fig. 2. Allowed multiple reflections for a range of φ and λ. Every point on this plot is exactly on the Bragg condition for the 200 reflection. The horizontal dashed line is where all measurements were made, and the other dashed lines represent multiple reflections involving a 222-type reflection. At those φ where a solid or dashed line intersects $\lambda/a_0 = 0{\cdot}312$, a multiple reflection will also exactly satisfy the Bragg condition.

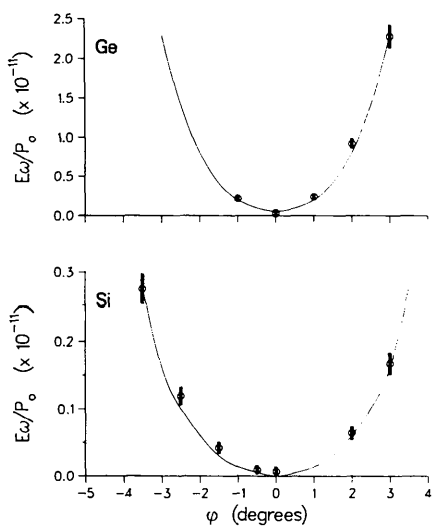

Fig. 3. Integrated intensity in the vicinity of $\varphi = 0°$. The circles are measurements and the curves are from 400-beam calculations. The error bars represent statistical uncertainty.

Table 1. *Integrated intensity* ($\times 10^{11}$) *of multiple reflections*

Ge				
φ(°)	0	34·795	16·565	
Calculated	0·058	2·5	26·0	
Measured	0·026	2·6	28·6	
Si				
φ(°)	0	19·5	20·0	34·825
Calculated	0·0	1·5	1·5	0·2
Measured	0·0068	1·712	1·699	0·2521

We made measurements of the integrated X-ray intensity at various φ angles, where φ is the angle between the plane of diffraction and the [010] direction. A schematic representation of this scattering geometry is shown in Fig. 1. Fig. 2 shows a plot of all possible multiple reflections for a range of φ values. The wavelength used is represented by the horizontal dashed line at $\lambda/a_0 \sim 0{\cdot}312$; the small arrows indicate the actual φ locations where X-ray scans were taken. Arrows below the line correspond to the location of silicon data, and arrows above the line to the location of germanium data. Those data that are clustered near $\varphi = 0°$ are plotted in Fig. 3, and the remainder are listed in Table 1.

IV. Results

In both Fig. 3 and Table 1 the measured data are shown with the results of 400-beam dynamical-theory calculations (Tischler & Batterman, 1986). These calculations are made on the assumption that $F_{200} = 0$ and they use published structure factors (Cromer & Mann, 1968) to compute the multiple-beam integrated intensities. Note that none of the data are scaled or fitted; both the measured and calculated intensities are absolute. The data points in Fig. 3 all lie very close to the calculated curves. A comparison of theoretical and experimental values shows that F_{200} must be smaller than $0{\cdot}0004 \pm 0{\cdot}00042$ electrons for silicon and $0{\cdot}00083 \pm 0{\cdot}00213$ for germanium.

At precisely $\varphi = 0$ we have a situation that is particularly convenient for measuring F_{200}. The multiple-beam contributions to the scattering amplitude add up to nearly zero, less than 0·003 electrons. Thus, most scattering that is observed can be directly attributed to F_{200}. The lack of any visible rocking curve at $\varphi = 0$ is a clear indication that F_{200} is extremely small. We located the correct 200 Bragg angle by simultaneously monitoring the 400 reflection at twice the energy.

V. Discussion

The sharp measured rocking curves show the scattered intensity peaked at the 200 node in reciprocal

space. Similarly, rocking curves calculated with dynamical theory show the contribution from each of the multiple beams peaked at the 200 node even though F_{200} is explicitly zero in the calculation. This feature of multiple-beam diffraction is also clearly shown by the δ functions present in the perturbation treatment of Shen (1986). The existence of sharp rocking curves does not require a non-zero structure factor, and multiple-beam effects are neither spread out in reciprocal space nor suppressed by a zero F_{200}.

A null F_{200} neither contributes to scattering nor suppresses the scattering from all of the other nodes in reciprocal space, even for nodes far from the Ewald sphere. At a randomly selected φ angle, one should expect measurable multiple-beam effects at the 200- and 420-type nodes in reciprocal space, even if F_{200} and F_{420} are zero. Also at the 622- and 442-type nodes, integrated intensities will, in general, differ from those predicted by the small but non-zero F_{622} and F_{442} (Tischler & Batterman, 1984). In both cases, ignoring the multiple-beam effects from nodes far from the Ewald sphere leads to inaccurate conclusions.

These results seem to explain the basis-forbidden reflection measurements of Post & Ladell (1987) that show a clear effect where the 311 and 002 nodes intersect the Ewald sphere. Just as many other multiple reflections were important at the 200 reflection examined in this work, the 'three-beam' case of 311 and 002 measured by Post & Ladell will also include many multiple-beam contributions. These extra contributions come from pairs of allowed reflections whose indices sum to 002, and must be included to calculate properly the diffracted intensity.

For the 200 measurements presented here, the narrow rocking-curve widths rule out surface diffraction as a possible source of error because surface peaks would be much wider. Harmonic contamination of the rocking curves can also be ruled out because any harmonic diffracting from the 400 reflection would remain constant with φ, whereas both the calculated and the measured integrated intensities approach zero at $\varphi = 0$ for our experimental conditions.

VI. Concluding remarks

We have shown that the 200 structure factor is zero within the experimental accuracy, and that all of the scattering intensity can be understood by performing multiple-beam calculations. Both the theoretical calculations and measurements show that easily measurable sharp rocking curves are to be expected at the 200 reflection and hence explain the observations of Post & Ladell (1987). It is important to note that the 200 integrated intensities are due to multiple-scattering contributions rather than a nonzero F_{200}.

References

CHAPMAN, L. D., YODER, D. R. & COLELLA, R. (1981). *Phys. Rev. Lett.* **46**, 1578-1581.

CROMER, D. T. & MANN, J. B. (1968). *Acta Cryst.* A**24**, 321-324.

DAWSON, B. (1967). *Proc. R. Soc. London Ser. A*, **298**, 255-263.

HENRY, N. F. M. & LONSDALE, K. (1952). *International Tables for X-ray Crystallography*, Vol. I, p. 341. Birmingham: Kynoch Press.

POST, B. & LADELL, J. (1987). *Acta Cryst.* A**43**, 173-179.

SHEN, Q. (1986). *Acta Cyrst.* A**42**, 525-533.

TISCHLER, J. Z. & BATTERMAN, B. W. (1984). *Phys. Rev. B*, **30**, 7060-7066.

TISCHLER, J. Z. & BATTERMAN, B. W. (1986). *Acta Cryst.* A**42**, 510-514.

Acta Cryst. (1988). A**44**, 25-33

On the X-ray Analysis of Thin Subsurface Layers. Bicrystal Diffraction Analogues

BY A. M. AFANAS'EV AND S. S. FANCHENKO

I. V. Kurchatov Institute of Atomic Energy, 123182 *Moscow, USSR*

(*Received* 30 *March* 1987; *accepted* 5 *August* 1987)

Abstract

X-ray determination of strain and damage distributions in thin subsurface layers from rocking curves is an ambiguous procedure. In the case of N distorted layers, all equivalent profiles can be obtained in the kinematical limit and their total number may be sufficiently large, being of the order of magnitude 2^N [Afanas'ev & Fanchenko (1986). *Dokl. Akad. Nauk SSSR*, **287**, 1395-1399]. A more detailed theoretical treatment of the problem and the analytical expressions of all bicrystal-equivalent crystal

0108-7673/88/010025-09$03.00